ACS EARTH AND SPACE CHEMISTRY

http://pubs.acs.org/journal/aesccq

Article

Reducing Conditions Influence U(IV) Accumulation in Sediments during *In Situ* Bioremediation

Noémie Janot,* Sarrah M. Dunham-Cheatham, Juan S. Lezama Pacheco, José M. Cerrato, Daniel S. Alessi, Vincent Noël, Eunmin Lee, Don Q. Pham, Elena Suvorova, Rizlan Bernier-Latmani, Kenneth H. Williams, Philip E. Long, and John R. Bargar

Cite This: *ACS Earth Space Chem.* 2024, 8, 148−158

Read Online

ACCESS | Metrics & More | Article Recommendations | Supporting Information

ABSTRACT: This study presents field experiments conducted in a contaminated aquifer in Rifle, CO, to determine the speciation and accumulation of uranium in sediments during *in situ* bioreduction. We applied synchrotron-based X-ray spectroscopy and imaging techniques as well as aqueous chemistry measurements to identify changes in U speciation in water and sediment in the first days follwing electron donor amendment. Limited changes in U solid speciation were observed throughout the duration of this study, and non-crystalline U(IV) was identified in all samples obtained. However, U accumulation rates strongly increased during *in situ* bioreduction, when the dominant microbial regime transitioned from iron- to sulfate-reducing conditions. Results suggest that uranium is enzymatically reduced during Fe reduction, as expected. Mineral grain coatings newly formed during sulfate reduction act as reduction hotspots, where numerous reductants can act as electron donors [Fe(II), S(II), and microbial extracellular polymeric substances] that bind and reduce U. The results have implications for identifying how changes in the dominant reducing mechanism, such as Fe versus sulfate reduction, affect trace metal speciation and accumulation. The outcomes from this study provide additional insights into uranium accumulation mechanisms in sediments that could be useful for the refinement of quantitative models describing redox processes and contaminant dynamics in floodplain aquifers.

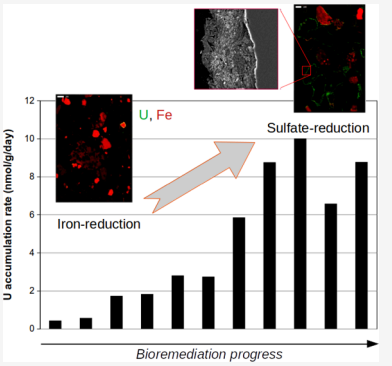

KEYWORDS: *bioreduction, sulfate, reducing conditions, uranium, metal, groundwater, X-ray spectroscopy*

INTRODUCTION

Uranium (U) is a radioactive element that can occur naturally in soils, minerals, and waters. Following the discovery of nuclear fission in the 1940s, its economic importance increased greatly and mining, energy, and military industries became anthropogenic sources of U in natural waters.[1] Existing remediation strategies include physical barriers or covers, plant uptake of radioelements, constructed wetlands, and abiotic or biotic strategies based on U reduction.[2,3] Indeed, reduced, tetravalent U [U(IV)] is considerably less soluble than the oxidized, hexavalent state [U(VI)], and consequently, reduction of aqueous U(VI) to insoluble U(IV) species is known to decrease its aqueous concentration.[1,4,5] Reduction of U(VI) to U(IV) can happen through biotic (e.g., bacteria enzymatically reducing uranium)[6,7] and abiotic [e.g., through Fe(II) species, that can be produced via microbial metabolism] processes.[8−10] Thus, to initiate reduction, contaminated groundwater can be amended with abiotic reductants, such as sulfide reagents or hydrogen gas, or with an electron donor (acetate, lactate) that stimulates microbial growth. The objective is to reduce U directly, enzymatically by the native microbial communities, or indirectly, by the formation of reduced compounds that reduce U abiotically, such as Fe(II) or sulfide species.[2] Initial expectations were the precipitation of U(IV) as crystalline uraninite (UO_2), which is a relatively stable product within the aquifer. However, laboratory and field experiments have shown the existence of non-crystalline U(IV) species,[9,11−14] which present less resistance to oxidation and mobilization than crystalline species.[15−17]

Research over past decades has greatly improved our understanding of biogeochemical processes governing U behavior in contaminated aquifers, thanks to interdisciplinary studies such as the studies conducted at the Rifle Integrated Field Research Challenge (IFRC) site in Colorado, U.S.A. At this site and others through the United States (e.g., Oak Ridge, TN, and Shiprock, NM), bioremediation approaches through electron donor amendment have been investigated at the field scale.[5,18−21] First, *in situ* bioremediation experiments at the Rifle site have shown that the addition of an electron donor to groundwater stimulates the growth of Fe(III) reducers (FRB),

Special Issue: Environmental Redox Processes and Contaminant and Nutrient Dynamics

Received: September 21, 2023
Revised: January 4, 2024
Accepted: January 4, 2024
Published: January 26, 2024

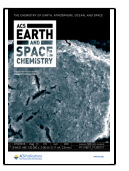

such as *Geobacter*, establishing iron-reducing conditions and removing U(VI) from solution. With time, sulfate-reducing communities (SRB) become predominant, creating reduced Fe−S phases that can also reduce U(VI).[5,19,22] The latest conceptual model of U bioreduction under dominant sulfate-reducing conditions suggests that U(VI) is reduced dominantly via a mixed abiotic−biotic pathway involving mackinawite (FeS) and aqueous sulfide (HS^-) as electron donors, and biomass [i.e., bacterial cells and extracellular polymeric substances (EPS)] as U-binding substrate.[28] Overall, it has been shown that biostimulation leads to substantial changes in aqueous chemistry, microbial community composition, and mineralogical changes, all of which impact the fate of U.[23,24]

To delineate the contributions of these various control factors and design a sustainable remediation strategy transferable to similar sites, it is necessary to develop numerical models describing the controlling reactions, their rates, and the associated reduced products. Initially, reactive transport models (RTMs) of bioremediation processes assumed only metabolic reduction by Fe-reducing bacteria, thus providing a lower absolute rate of U(VI) bioreduction under sulfate-reducing conditions than under Fe-reducing conditions.[23,25,26] More recently, abiotic reduction of U(VI) by FeS has been included in a RTM to describe the variation of U isotopic ratios measured during a bioremediation experiment at Rifle.[27] These numerical models have been parametrized and/or validated using aqueous measurements [primarily, Fe(II), sulfate, and U(VI) concentrations], making it difficult to quantitatively discern the individual contribution of processes governing these concentrations as a result of the numerous intricate reactions of various rates governing the biogeochemistry of these elements.[23] Indeed, the release of dissolved Fe(II) and sulfides by Fe(III)- and sulfate-reducing processes can lead to the precipitation of FeS minerals, affecting the dissolved Fe(II) and sulfide concentrations and our ability to quantify the rate of Fe(III)- and sulfate-reducing processes from aqueous measurements alone.

Solid-phase analysis of subsurface sediment samples, in addition to aqueous measurements, can help to better constrain these models. In-well, flow-through columns, packed with sediments and installed in the aquifer that can be harvested at various time points during a field experiment, are an effective approach to gain access to these products.[22,28] Using such a design, field experiments performed at the Rifle site by our group in 2009 and 2010 showed no change in U(IV) products formed in sediment after 24−90 days of acetate amendment (i.e., under iron to sulfate reduction), with data showing that the majority of reduction products were biomass-bound, non-crystalline U(IV) species under all conditions studied.[22,28] Indeed, these various reduction pathways have been shown to produce similar U(IV) products,[29−33] making it difficult to discriminate between the various processes and determine the rates of the controlling reactions. Additional approaches combining Fe, S, and U behavior in solid and aqueous fractions are needed to discriminate between reduction mechanisms controlling the rate of U accumulation.

Here, we investigate the impact of the main biogeochemical regime on U(IV) accumulation over the course of bioreduction experiments from the early Fe reduction stages to the transition to sulfate-reducing conditions. Using in-well columns, our investigation integrated field experiments, aqueous chemistry measurements, solid synchrotron-based X-ray absorption spectroscopy, and spatially resolved fluorescence mapping to constrain U(VI) reduction mechanisms during bioremediation. This time-resolved study provided samples from which accumulation rates of U(IV) can be calculated, data that are critical to parametrize RTMs. The novelty of this study lies in the measurement of the increase of the U(IV) accumulation rate with the onset of sulfate-reducing conditions in field experiments, corresponding to the appearance and accumulation of FeS grain coatings acting as U reduction hotspots. This field experimental study identifies the co-evolution of Fe, S, and U biogeochemistry in the solid phase, which is needed to constrain conceptual and numerical models of U dynamics in contaminated floodplain aquifers.

METHODS

Site Description and *In Situ* Field Experiment. Description of the Rifle IFRC site and its bioremediation experiments have been published elsewhere.[5,19,23] Details of sediment and groundwater composition are given in Table S1 and Figure S1 of the Supporting Information. Here, in-well experiments were conducted using a design similar to those reported by Bargar et al.[28] and Alessi et al.[22] Nine column reactors were operated during a larger uranium bioreduction field experiment in August 2011 in the experimental plot C well gallery of the Rifle IFRC site described by Williams et al.[5] and Long et al.[23] (Figure S2 of the Supporting Information). Rifle area background sediment (RABS) was harvested from below the water table in an area not impacted by previous bioreduction experiments, wet-sieved to <2 mm, and immediately loaded into glass chromatography columns (2.6 cm diameter, 15 cm length, and approximately 150 g of sediments). As a result of the high number of reactors, columns had to be installed in two neighboring groundwater wells, CD-07 and CD-08. Installations were made on August 6−8, 2011, and groundwater was then pumped through the reactors at a flow rate of 1 mL min^{-1} (corresponding to ≈60 pore volumes day^{-1}) to recondition the sediments to groundwater chemical composition and microbial communities (Figure S3 of the Supporting Information). The addition of acetate for the field-scale bioremediation experiment in the aquifer started on August 23, 2011 (groundwater concentration of approximately 15 mM) from wells located ∼8 m upgradient from the location of our reactors.[34] Acetate was detected in groundwater of wells CD-07 and CD-08 on September 9, 2011 (Figure S4 of the Supporting Information). Thus, on this day, referred to in this study as day 0, reactor influent groundwater was directly amended with 12 mM acetate and 6 mM bromide as a tracer, at a flow rate of 1 mL min^{-1} to initiate reducing conditions in the reactor sediments. On day 12/13, the amendment was paused and the reactors were flushed with anaerobic groundwater from a nearby well not affected by the field amendment, to remove excess Fe(II) in solution. This step was needed to avoid direct abiotic U reduction during the next step and have access to U(IV) products of bioreduction. On day 17, the amendment started again, with an addition of 10 μM U(VI) to the influent solution, significantly higher than the background U(VI) concentration in the Rifle aquifer groundwater (<ca. 1 μM). This additional U(VI) was needed to ensure that final concentrations in the sediments would be amenable for spectroscopic analysis while being representative of historical U(VI) concentrations found at contaminated sites within the Colorado River basin (<ca. 50 μM).[22]

https://doi.org/10.1021/acsearthspacechem.3c00271
ACS Earth Space Chem. 2024, 8, 148−158

Table 1. Experimental Parameters for *In Situ* Reactors of the 2011 Experiment

manuscript reactor name		R1	R2	R3	R4	R5
field reactor name		1A	1D	1I	2EFHIJ	1J
well		CD-07	CD-07	CD-07	CD-08	CD-07
preconditioning groundwater elution duration (day)		31	31	31	33	31
reactor amendment (12 mM acetate)	start (day number)			0		
	duration (day)	13	13	12	12	13
"Fe" flush duration (day)		4	4	5	5	4
reactor amendment (12 mM acetate/10 μM uranyl)	start (day number)			17		
	duration (day)	5	8	11	15	22
GW flush duration (day)		5	5	5	8	10
harvest day		27	30	33	39	49
dominant biogeochemical regime (on the basis of aqueous data)		Fe red.	Fe red.	Fe red.	Fe red.	SO_4 red.

The reactors were harvested after different periods of amendment, from 5 to 22 days, designated as R1−R5 (Table 1). Before harvest, the influent was stopped and the reactors were eluted with in-well groundwater for 5−10 days to flush out unreduced U(VI). During harvest, inlet/outlet lines were closed with end caps to isolate the sediment from the atmosphere. Within 5−10 min, the entire intact reactors were placed in stainless-steel shipping containers and purged with N_2 gas. Harvested reactors were sealed under anoxic conditions with a slight positive N_2 pressure to prevent O_2 entrance into the containers and shipped overnight to the Stanford Synchrotron Radiation Lightsource (SSRL) or Washington University in St. Louis (WUStL) for further analysis. Upon arrival at the lab, reactors were opened in an anaerobic chamber (5% H_2/balance N_2) and sediments were subsampled in four parts in stoppered serum bottles named from top (effluent) to bottom (influent): top1, top2, bot1, and bot2. Until analysis, the serum bottles were stored frozen in anaerobic jars to slow further biogeochemical reactions. In the subsequent analysis, top1 and top2 samples were mixed to form the "top" sample of the reactor, and bot1 and bot2 were mixed and labeled "bottom".

Sample R4 was obtained by homogenizing five reactors amended concurrently under the same conditions and harvested together. Reactor sediments were mixed and subsampled for time point R4. The rest of the material was reinstalled in reactors in the aquifer for a subsequent aging experiment.

Aqueous Chemistry of Effluent Solutions. Reactor effluents were sampled at least twice a week and analyzed to determine the aqueous concentrations of U(VI), bromide, sulfate, sulfide, and acetate. Groundwater samples were also collected from wells CD-07 and CD-08 several times per week during the experimental period. Details of the analytical methods can be found in the study by Williams et al.[5] Briefly, acetate, bromide, and sulfate were measured using an ion chromatography system (ICS-1000, Dionex, CA, U.S.A.) equipped with an AS-22 column. Aqueous sulfide, Fe [Fe(II) and total Fe], and dissolved oxygen were quantified on site using spectrophotometry (CHEMetrics field test kits). Dissolved uranium was quantified using kinetic phosphorescence analysis (Chemchek Instruments, Richland, WA, U.S.A.).

Complementary Samples. Samples from reactors run during the 2010 field experiment, harvested under a wider range of redox conditions, were used for a complementary analysis and comparison. They are labeled T1 (corresponding to Fe reduction), T2 (early sulfate-reducing conditions), and T3 (late sulfate-reducing conditions). Detailed information about their composition and history can be found in the study by Alessi et al.[22] and Table S2 of the Supporting Information.

Chemical Extractions. All chemical extractions were conducted in triplicate, and reactors consisted of ∼1 g of sediment reacted with 25 mL of extractant solutions in 50 mL Teflon digestion tubes. The non-crystalline U(IV) fraction was determined by a bicarbonate extraction using a method described in detail in the study by Alessi et al.[35] Briefly, in an anaerobic chamber, ∼1 g of dried sediment was mixed with oxygen-free 1 M bicarbonate solution for 24 h. The acid-extractable elemental content of U and Fe in sediments was determined by reaction with aqua regia, comprised of a 1:4 (v/v) mixture of HCl (34−37% by mass, trace metal grade) and HNO_3 (67−70% by mass, trace metal grade). A volume of 5 mL of aqua regia was added to 20 mL of deionized water to reach a final extractant solution volume of 25 mL in each reactor; all reactors were placed in a heated digestion block at 100 °C for 4 h. Another acid extraction was conducted by reaction with 0.25 M HCl for 30 min to measure readily extractable Fe.

Aliquots of the extraction solution were acidified and filtered through 0.45 μm pore size membranes [polytetrafluoroethylene (PTFE), Millipore]. Aqueous filtrates were diluted in solutions of 2% HNO_3, and U and Fe were quantified using inductively coupled plasma mass spectrometry (ICP−MS, Agilent 7500ce).

X-ray Fluorescence Spectrometry (XRF) Analysis. Bulk sediments were ground, and a 3 g subsample of powdered sediments was analyzed for total chemical compositions using XRF with a SPECTRO XEPOS energy-dispersive X-ray fluorescence spectrometer equipped with a Pd cathode and operating at 50 kV and 40 mA at the Stanford Environmental Measurements Facility. Each concentration was an average of three analyses and was quantified using the supplier-provided software and the NIST 2711 certified reference material that was intercalated during the analytical series.

X-ray Absorption Spectroscopy (XAS). *U L_{II}-Edge XAS Data Collection.* Uranium L_{II}-edge fluorescence yield XAS spectra were measured at beamline 11-2 at SSRL. The U L_{II}-edge was preferred to the U L_{III}-edge to avoid interference of the U Lα fluorescence peak (13 614 eV) with the rubidium fluorescence Kα peak (13 396 eV). The samples were loaded in an Al sample holder with Kapton windows inside an anaerobic chamber (2−5% H_2 with balance N_2). Immediately prior to analysis, the sample was mounted in a liquid N_2 cryostat, placed under a vacuum, and cooled to 77 K. A Si(220) double-crystal monochromator was detuned 15−30%

https://doi.org/10.1021/acsearthspacechem.3c00271
ACS Earth Space Chem. 2024, 8, 148−158

to reject higher harmonic intensity. Fluorescence yield spectra were collected using a 100 pixel germanium X-ray detector. Energy calibration was monitored continuously using a Mo foil in a double-transmission setup.

S K-Edge X-ray Absorption Near-Edge Structure (XANES) Data Collection. S K-edge XANES spectra were collected at SSRL beamline 4-3 using a double-crystal Si(111) monochromator. Samples were ground in an anaerobic chamber before analysis. The samples were pressed in Al holders using S-free tape and covered with a polypropylene film. Spectra were collected under a He atmosphere at room temperature in fluorescence mode using a Vortex detector. X-ray energy was calibrated to the K-edge of sodium thiosulfate (2472 eV). Scans were collected from 2420 to 2700 eV with a step size of 0.15 eV around the edge. Each XANES spectrum was composed of an average of 3−6 scans. No beam damage was detected, and self-absorption was considered to be insignificant because most samples were fine-grained with S concentrations below 2%.[36]

XAS Data Analysis. S K-edge and U L_{II}-edge XANES and U L_{II}-edge extended X-ray absorption fine structure (EXAFS) spectra were background-subtracted, splined, and analyzed using the SixPack[37] and DEMETER suite[38] software packages.

S K-edge XANES spectra were analyzed by linear combination fitting (LCF) in Larch software[39] between 2466 and 2484 eV. Model compounds were selected among potassium sulfate (K_2SO_4), anhydrite ($CaSO_4$), sodium thiosulfate ($Na_2S_2O_3$), synthetic polysulfides, elemental sulfur [$S(0)^6$], pyrite (FeS_2), synthetic mackinawite [$Fe_{(1+x)}S$], mackinawite exposed to sub-stoichiometric amounts of weak oxidants or Fe^{3+} (referred to as oxidized mackinawite), and greigite (Fe_3S_4), as described in the study by Noël et al.[40] Only the most significant compounds were kept for final analysis: sulfate as K_2SO_4, elemental sulfur, and oxidized mackinawite.

U L_{II}-edge XANES were fitted between 20 916 and 21 016 eV, using andersonite [$Na_2Ca(UO_2)(CO_3)_3{\cdot}6H_2O$, U(VI)] and biogenic uraninite U(IV) as model compounds.[41] U L_{II}-edge EXAFS spectra were fitted as $\chi(k)$ between 2 and 9 $Å^{-1}$, using biogenic uraninite and non-crystalline U(IV) as reference spectra.[11]

The quality of the fits was estimated by the following *R*-factor parameter of the following form: $R_f = \sum[k^3\chi(k)_{exp} - k^3\chi(k)_{calc}]^2/\sum[k^3\chi(k)_{exp}]^2$. The accuracy of the fitting procedure is estimated to be ±5% of the fit-determined *R*.[42] The components below 5% are thus considered as not significant.

Microscopy Analysis. *Thin-Section Preparation.* Sediments were dried and embedded in degassed epoxy (EpoTek 301) in an anaerobic chamber (3−5% H_2 with balance N_2). Petrographic thin sections were prepared by Spectrum Petrographics, Vancouver, WA, U.S.A., and stored anaerobically when not analyzed.

X-ray Microscopy. The full petrographic thin sections were initially mapped at SSRL beamline 10-2 (25 μm spot), at 17 120 eV. X-ray microprobe images and μ-XAS spectra at U L_{III}-edge were collected at SSRL beamline 2-3 (2 μm spot, 50−250 ms dwell time, and vortex fluorescence detector). Difference and tricolor maps were calculated using the MicroAnalysis Toolkit software.[43] Measurements were performed at room temperature. The angle subtended by the incident beam, sample, and detector was 90°, with the sample normally bisecting this arrangement.

Scanning Electron Microscopy (SEM)/X-ray Energy-Dispersive Spectrometry (EDS) Analysis. SEM and EDS were performed on a Carl Zeiss MERLIN (Oberkochen, Germany) microscope at 3−10 kV accelerating voltage in secondary electron imaging mode for sediment grain imaging and chemical analysis. Quantification of elements was performed using an INCA X-ray EDS system (Oxford). SEM micrographs were collected from more than 80 individual grains, and from those, EDS measurements of elemental composition were made on more than 350 individual points.

RESULTS AND DISCUSSION

Timing the Transition from Iron- to Sulfate-Reducing Conditions from Aqueous Measurements in Whole Sediment Reactors. During the 2011 field amendment experiment (the second stimulation in the experimental plot C well gallery of the Rifle IFRC), the onset of sulfate-reducing conditions, operationally evidenced by the decrease of the sulfate concentration and the appearance of sulfide in the groundwater, was seen from day 15 in both wells CD-07 and CD-08 (Figure S4 of the Supporting Information). This expected evolution was observed much sooner than in the 2010 experiment, when iron-reducing conditions were still dominant after 24 days of amendment.[22] Previous biostimulation studies showed that acetate amendment to the Rifle aquifer leads to the development of iron-reducing conditions, followed by sulfate-reducing conditions.[5,19,22] However, the timing of this shift is modified upon subsequent stimulation experiments; indeed, a legacy effect has been documented, leading to earlier sulfate-reducing conditions when the aquifer has been previously amended with electron donors.[44,45] With this study, we were thus looking at the transition from dominant iron-reducing conditions (in reactors R1−R4) to dominant sulfate-reducing conditions (in reactor R5), operationally characterized by the consumption of all aqueous sulfate.

The evolution of dissolved U(VI), acetate, bromide, and sulfate concentrations over the course of the experiment is shown in Figures S6−S10 of the Supporting Information (for R1−R5). Results show that the acetate groundwater concentration in well CD-07 was ≤8 mM, whereas in well CD-08 it was ≤4 mM, leading to greater U(VI) and sulfate removal in CD-07 than in CD-08, in both the groundwater and the reactors installed there (Figures S4 and S6−S10 of the Supporting Information). Thus, on the same day, the biogeochemical conditions were different in the neighboring wells, which *a priori* makes the comparison of time-resolved results from reactors coming from different wells difficult. Accordingly, care should be taken regarding the interpretation of the results from reactor R4.

Uranium Accumulation in Sediments. The solid-phase uranium concentration in the bioreduced sediments increased with time and ongoing remediation (Figure 1). Reactor R5, harvested under dominant sulfate-reducing conditions, was greatly enriched in uranium compared to the others. The effluent (top) part of reactor R2 was significantly enriched in uranium compared to the bottom of the same reactor or compared to samples from reactors R1−R3. With this result being incoherent with the general increase of the U concentration with time and the observation previously made in similar setups that U concentrations are higher at the inlet end of the column (i.e., bottom) than at the outlet end, it may thus be considered as an outlier. This may be due to

https://doi.org/10.1021/acsearthspacechem.3c00271
ACS Earth Space Chem. 2024, 8, 148−158

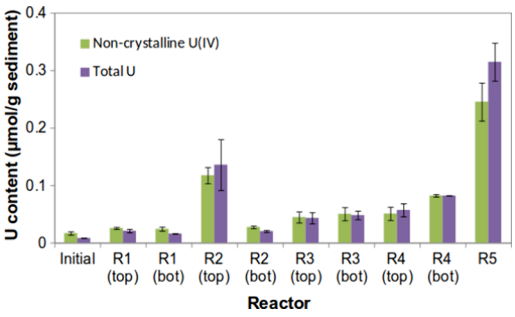

Figure 1. Evolution of the uranium content with ongoing bioreduction, as quantified by chemical extractions: bicarbonate-extracted non-crystalline U(IV) species (green bars) and total U from total digestion (purple bars), reported in micromoles of U per gram of sediment. Error bars represent the error from triplicate measurements.

preferential flow path that had formed inside the column or low effluent flow rate requiring a change of effluent pump tubing during the last flush. It will thus not be considered in the following discussion.

XANES spectra indicated that U was present as 100% reduced U(IV) in all reactors, except R1 (bot), for which LCF indicated a small (4%) contribution of U(VI) as andersonite (Figure S11 of the Supporting Information), which is not significant because it is lower than the detection limit of the method.[41] Chemical extractions showed that, for all cases, most U in the sediments was bicarbonate-extractable, suggesting the predominance of non-crystalline U(IV) (Figure 1). Some UO_2 might have formed after 22 days (R5), as indicated by slight differences in the U concentration obtained by total digestion compared to bicarbonate extraction.

EXAFS spectra were recorded for the most concentrated samples (R2 top, R3 bot, and R5). They were similar despite the noise as a result of the low total U concentration (less than 80 μg/g) (Figure 2), and results of the EXAFS analyses agreed

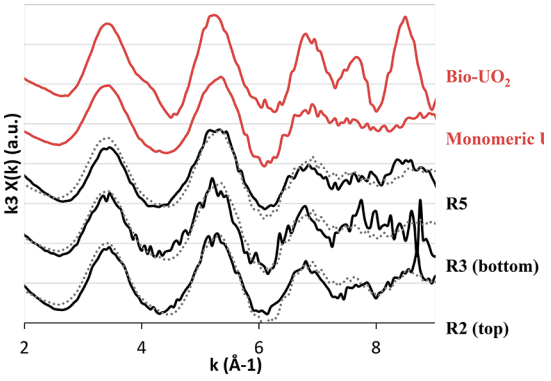

Figure 2. U L_{II}-edge EXAFS spectra of the reactor sediments (black) and reference species (red). Data are in plain lines, and LCF results are in dotted gray lines.

with the macroscopic quantification. LCF of the EXAFS spectra between 2 and 9 $Å^{-1}$ using crystalline biogenic UO_2 and non-crystalline (monomeric) U(IV) as standards gave estimates of 83, 95, and 94% of non-crystalline U(IV) in samples R2 top, R3 bot, and R5, respectively (Figure S11 of the Supporting Information). All magnitudes of Fourier transform spectra showed a U−P/C shell at ca. 2.9 Å that was consistent with non-crystalline U(IV) associated with biomass as well as a U−U pair correlation at ca. 3.7 Å, implying the presence of uraninite (Figure S12 of the Supporting Information). These results agree with results from the 2010 experiment; however, the proportion of uraninite in 2010 reactors was greater and reached $^1/_3$ of U(IV) accumulated under late iron reduction as well as under sulfate reduction.[22] This may be due to a higher incoming U(IV) concentration in the 2010 experiment, changing the surface/U ratio of the system.[30,32,46]

Rates of uranium reduction are known to be controlled by its aqueous speciation[29,47] but also by various processes of desorption, bioreduction, and precipitation.[13,48] It is not easy to decipher the main mechanisms observed in natural sediments in field experiments. Here, U accumulation rates in the different reactors were calculated depending upon the duration of uranium amendment by dividing U accumulated in the sample (U content in the sample corrected from the U content in the initial material, in nmol g^{-1}) by the duration of reactor acetate amendment (days). Results are shown in Figure 3, plotted together with data from reactors operated during the earlier 2010 "Super 8" experiment[22] and the 2009 "Buckskin" experiment.[28] Corresponding numerical values can be found in Table S1 of the Supporting Information.

Despite varying concentrations of acetate and U in the amendment solutions, the results show consistent trends between data from experiments performed in different years. In early samples, harvested under Fe reduction, U accumulated at 0.5−2 $nmol_U\ g^{-1}{}_{sediment}\ day^{-1}$. Once sulfate-reducing conditions became predominant (starting between 27 and 33 days of amendment in all experiments), accumulation rates were higher, from 6 and up to 10 $nmol_U\ g^{-1}{}_{sediment}\ day^{-1}$, with the difference being the highest at the bottom of the reactors. It is difficult to quantitatively compare these values to U(VI) reduction rates published in the literature, because field-based rates are always smaller than the rates observed in laboratory systems.[49] However, the increase in the accumulation rate with ongoing bioremediation observed here is in agreement with previous results on bioreduction experiments in sediment columns in the lab,[50] in which the authors observed an increase of the biomass concentration in the presence of sulfate reduction, thus leading to a higher number of electrons transferred. Our results also coincide with observations made by Long et al. during the 2010 field bioremediation experiment in the Rifle aquifer. These authors observed a sharp increase of the biomass amount, particularly of sulfate reducers, after 30−35 days of acetate amendment and estimated from aqueous data a simultaneous increase of U(VI) bioreduction rates.[23] Our data set supported this hypothesis, confirming a higher uranium accumulation rate under predominantly sulfate-reducing conditions.

In addition to the increase in the biomass concentration, sulfate-reducing conditions also affected the speciation of Fe and S, also impacting the uranium-reducing mechanisms and subsequent accumulation rate. Behrends and van Cappellen studied enzymatic and abiotic U(VI) reduction mechanisms under Fe-reducing conditions in closed systems and showed that abiotic reduction leads to higher U(IV) accumulation rates than pure biotic processes.[51] The change in the accumulation rate observed here could be a result of a change in the main reduction processes. Indeed, during sulfate reduction, the generation of aqueous sulfide and the precipitation of mackinawite create abiotic reduction pathways that do not exist under Fe-reducing conditions.[10] Fe and S

https://doi.org/10.1021/acsearthspacechem.3c00271
ACS Earth Space Chem. 2024, 8, 148−158

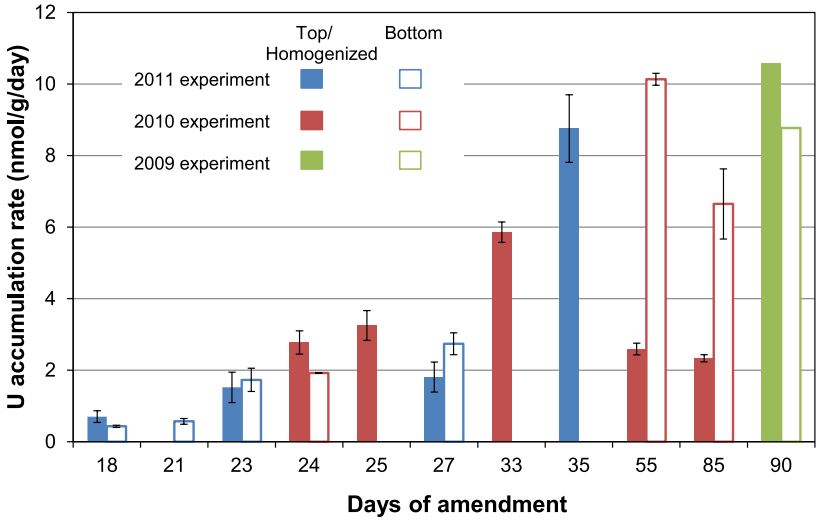

Figure 3. Uranium accumulation rates in the reactors during different field experiments (Buckskin 2009 in green, Super 8 2010 in red, and Best Western 2011 in blue), depending upon the duration of the column amendment. The 2010 and 2009 rates were calculated from data published in the studies by Alessi et al. and Bargar et al., respectively.

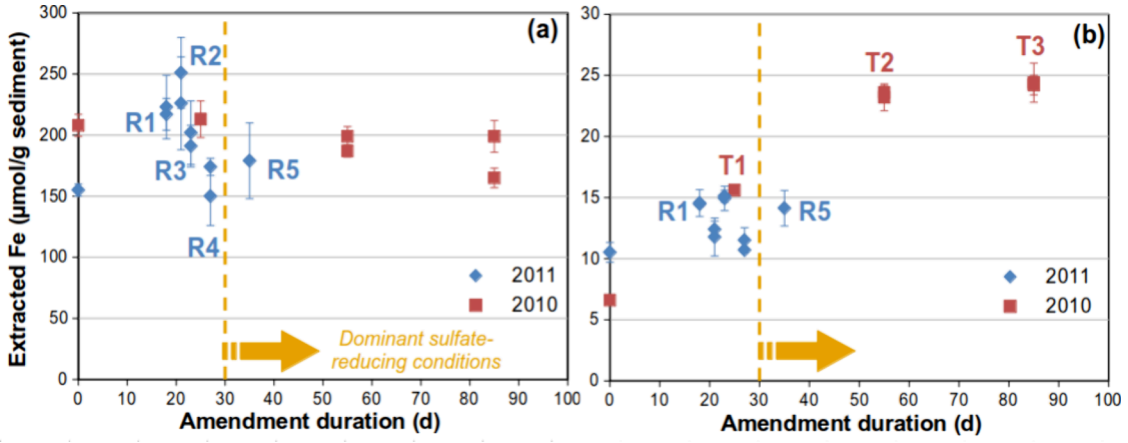

Figure 4. Fe content as determined by HCl extractions, including (a) total digestion and (b) after 0.5 h, performed on reactor sediments as a function of the amendment duration for 2011 (R1−R5, blue diamonds) and 2010 (T1−T3, red squares) field experiments.

solid speciations during the experiment were analyzed to test and support these hypotheses.

Evolution of Bulk Solid Biogeochemistry during Bioreduction. Sediments became darker with ongoing bioremediation, especially after the onset of sulfate-reducing conditions, suggesting the precipitation of iron sulfide minerals (mackinawite FeS, greigite Fe_3S_4, and pyrite FeS_2), as shown previously.[22] Results of Fe extraction evidence few differences in extractable Fe contents with time or location in the columns (Figure 4a), suggesting that there was no loss of total iron with ongoing reduction. However, we did observe an increase in the most readily extractable fraction (0.5 h) with time, especially during the 2010 experiment under predominant sulfate-reducing conditions (reactors T2 and T3; Figure 4b), which can be related to an increase in the amount of poorly crystallized Fe phases in sediments.[52]

The sulfur content in the reactors, combined with S speciation as determined by sulfur K-edge XANES analysis, is shown in Figure 5. Initially, all solid S in the sediment was present as sulfate. S started to accumulate in the sediments from the first time points, even under dominant Fe-reducing conditions, as elemental sulfur. This S^0 pool was observed for the entire duration of the experiment. It can be produced by the abiotic reduction of Fe^{3+}, reacting with aqueous sulfide (H_2S) according to the following reaction:[27,44]

$$2Fe^{3+} + H_2S_{aq} \rightarrow 2Fe^{2+} + 2H^+ + S^0$$

Accordingly, S accumulates as S^0 in early samples, because sulfide was already detected in the well groundwater once U amendment in the reactors started (Figures S4−S6 of the Supporting Information).

After 23 days of acetate amendment (reactor R3), the predominant reaction is sulfidation and mackinawite (FeS) appeared in the sediments. It became the major S phase in all reactors harvested after 27 days of amendment (Figure S13 of the Supporting Information and corresponding values in Table S3 of the Supporting Information), evidencing the predominance of sulfate-reducing conditions. Using this percentage of S present as FeS to discriminate the main biogeochemical regime, it seems that sulfate-reducing conditions were also dominant in reactor R3 (Figure S13 and Table S2 of the Supporting Information). The S^0 amount increased again in late sulfate-reducing conditions (reactor T3 from the 2010

https://doi.org/10.1021/acsearthspacechem.3c00271
ACS Earth Space Chem. 2024, 8, 148−158

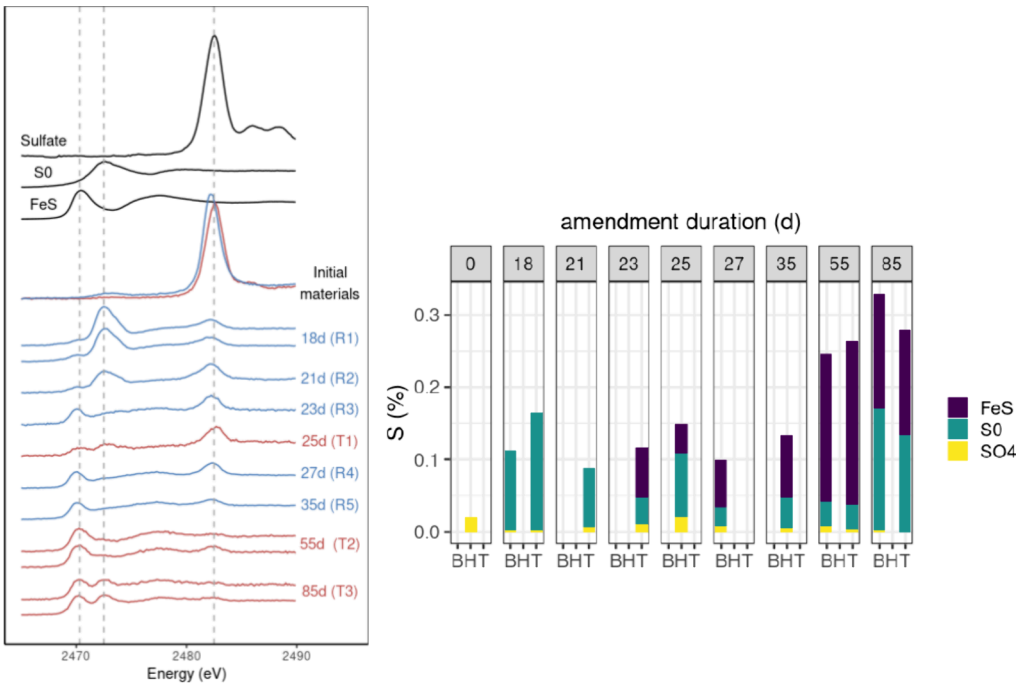

Figure 5. Representative bulk S−K edge XANES spectra of samples from 2010 (in red) and 2011 (in blue) field experiments (left) and quantitative S speciation in the reactors (bottom B, top T, or homogenized H) harvested after various durations of acetate amendment (right). Results were obtained from LCF fitting analysis of XANES and XRF measurements.

experiment), which may be related to the abiotic reduction of $U^{(VI)}$ by freshly formed FeS as follows:

$$FeS_{am} + UO_2^{2+} + 4H^+ \rightarrow Fe^{2+} + S^0 + U^{(IV)} + 2H_2O$$

These measurements showed that the entire pool of solid S is modified with ongoing bioremediation, which can help resolve the dominant biogeochemical regime. The increase in the accumulation rate of uranium in late reactors can be related to the predominant sulfidation in corresponding sediments.

Evolution of Grain-Scale Dynamics with Time. SEM and microprobe analysis of the initial material showed mainly SiO_2 grains with no coatings as well as some Fe oxide grains, some with Al−K silicate inclusions (Figure 6a and more on Figure S14 of the Supporting Information). In column T1 from the 2010 experiment, harvested under late Fe reduction, limited coatings were observed. SEM/EDS measurements around one grain showed aluminosilicate coatings locally enriched in Fe (up to 20 wt %; see Figure 6). Under predominant sulfate-reducing conditions, when sulfidation is the main mechanism of S reduction, we observed well-developed coatings around quartz and iron oxide grains (panels c and d of Figure 6). More examples are shown in Figures S15 and S16 of the Supporting Information.

In the 2010 experiment, we observed a progressive increase in the S content in these coatings with ongoing bioremediation, as shown in Figure 6e. The initial material as well as T1 do not show any S accumulation in the grain coatings. However, when sulfate reduction became predominant (reactors T2 and T3), S accumulated around sediment grains, until a 1:1 Fe/S correlation was observed in the influent end of column T3, confirming the precipitation of mackinawite. In this sample, 127 measurements were made at grain boundaries, and Fe and S were co-present in 101 of these points (80%).

However, U distribution within these coatings was highly heterogeneous, with 45 out of 127 coating spots analyzed by

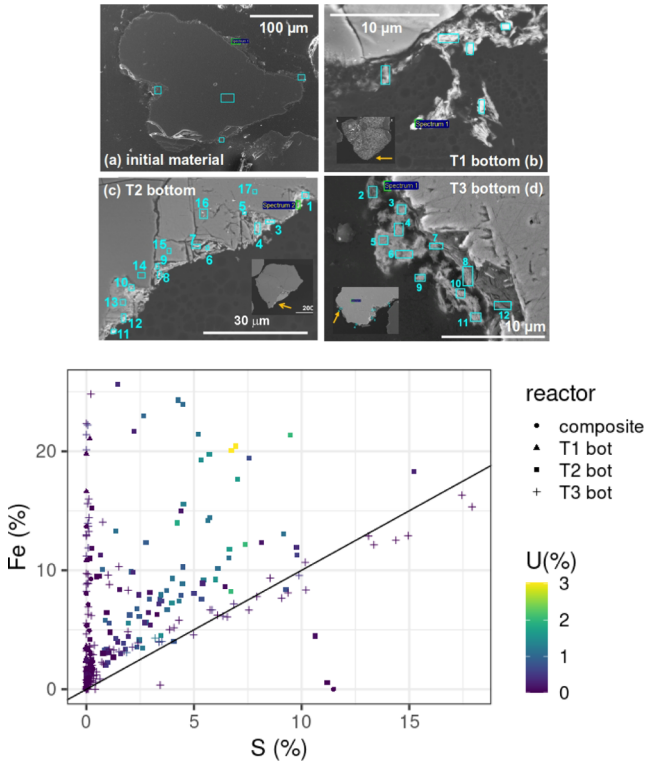

Figure 6. (a−d) SEM micrograph of quartz grain coatings from the 2010 reactors and (e) Fe and S atomic percent in grain coatings from SEM/EDS data for the inlet of T1−T3 reactors from the 2010 experiment as well as the initial material. The line corresponds to the 1:1 Fe/S correlation. The color of the symbols represents the corresponding U atomic percentage.

EDS in reactor T3 showing no detectable U. Moreover, the highest U concentrations were not found in the same spots as

https://doi.org/10.1021/acsearthspacechem.3c00271
ACS Earth Space Chem. 2024, 8, 148−158

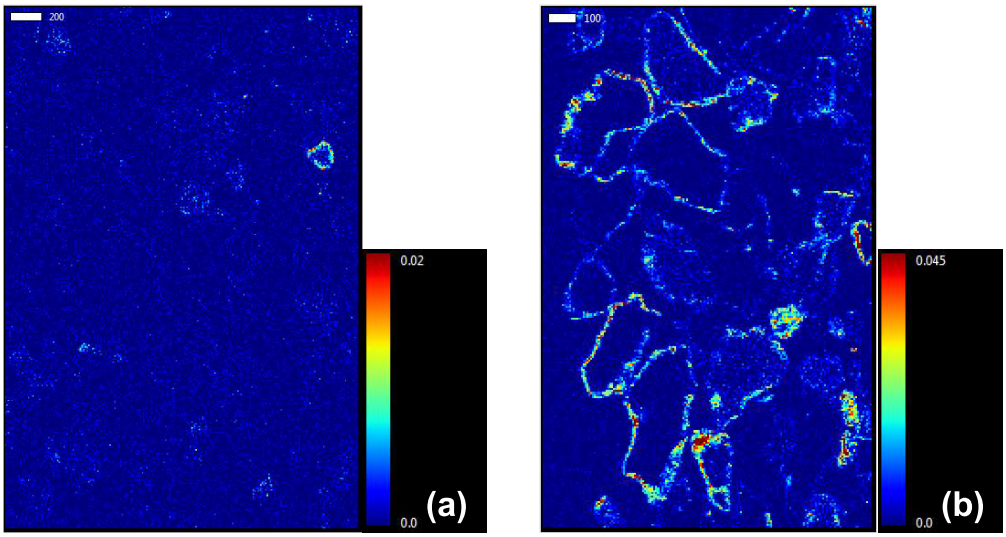

Figure 7. X-ray U fluorescence maps in sediments harvested under (a) iron reduction (reactor T1 from 2010 experiment) and (b) sulfate reduction (T3), together with a color legend in arbitrary units.

FeS (Figure 6e). These observations support a strong biological role in U reduction. These coatings indeed concentrate bacteria in biofilms, in agreement with previous studies that showed that the transition from Fe- to sulfate-reducing conditions was accompanied by a decline in planktonic metal reducers and an increase in sessile cells and sulfate-reducing bacteria, such as *Desulfotomaculum* and *Clostridium* that are expected to be mainly mineral-attached.[23,28,53] These microbes concentrate many products that can bind and reduce U, thus acting as reduction hotspots.

Elemental distribution maps were measured using X-ray microscopy on thin sections from samples from the 2010 field experiment.[22] Results corroborate SEM/EDS observations showing the change in pore-scale distribution of U between predominantly Fe- and sulfate-reducing conditions (panels a and b of Figure 7, respectively). We observed at the grain scale that U is mostly diffusely distributed throughout the sediment under iron reduction, when it concentrates in grain coatings developed under sulfate reduction, as previously demonstrated.[22,28]

CONCLUSION

Various *in situ* bioreduction field experiments performed by our group in the Rifle aquifer provide consistent results. First, the bulk speciation of uranium is composed mainly of non-crystalline U(IV) and does not change with time and major biogeochemical conditions. This agrees with previous observations showing that non-crystalline U(IV) species are expected when microbial exopolymers and reducing agents are present, independently from the total U concentration or redox conditions.[12,22,46]

However, here, we observed measurable changes in the U accumulation rate and pore-scale distribution over the course of *in situ* bioreduction experiments. Under dominantly sulfate-reducing conditions, U was concentrated in grain coatings and its accumulation rate sharply increased. These grain coatings, previously observed by Bargar et al.[28] and Alessi et al.,[22] concentrated the biomass as well as various reductants, such as Fe(II) or aqueous sulfide. These fresh phases thus play the role of "reduction hotspots" that accelerate overall accumulation rates of U(IV) in the bioreduced sediments.[46] With this new information, we can refine existing models of U bioreduction in which aqueous U(VI) primarily undergoes enzymatic reduction by planktonic bacteria under Fe-reducing conditions. Subsequently, when sulfate-reducing conditions develop in the sediments, grain coatings develop and U(VI) binds to the newly formed phases (EPS and FeS)[12,28] that are composed of various reductants [microbes, Fe(II), and S(II)]. Reduced U(IV) then binds to the various ligands located in these coatings. Our observations agree with observations made by Bone et al. in organic-rich natural substrates in conditions similar to the Rifle aquifer[46] as well as by Mikutta et al.[53] in peatland samples, suggesting that surface complexes can inhibit uraninite formation.

This information is essential to better describe the uranium behavior in aquifers during bioremediation experiments. Illustrating the importance of the nature of reducing mechanisms and the grain-scale dynamics over aqueous data, this study also provides experimental data that can constrain and parametrize existing RTMs of contaminants within the subsurface.[27] RTMs should assume that remediation efforts generating biogeochemical conditions similar to those of this study will result in the formation of non-crystalline forms of U(IV) that are inherently more susceptible to reoxidation and remobilization. Subsequent RTM development should include information on the U accumulation rate and the corresponding U(IV) solid speciation, because the success of bioremediation lies in the stability of the U products accumulated over time and particularly their resistance to reoxidation that can occur when the water table decreases during the warm season. New knowledge provided by our study shows that it is critical to establish sulfate-reducing conditions in *in situ* bioremediation to achieve efficient accumulation of uranium.

ASSOCIATED CONTENT

Supporting Information

The Supporting Information is available free of charge at https://pubs.acs.org/doi/10.1021/acsearthspacechem.3c00271.

Details on the field site and bioreduction experiment, including groundwater and reactor effluent concentrations and calculation of U accumulation rates

https://doi.org/10.1021/acsearthspacechem.3c00271
ACS Earth Space Chem. 2024, 8, 148−158

(Appendix S1), uranium XANES and EXAFS spectra (Appendix S2), and SEM and microprobe Fe−U maps of 2010 samples (Appendix S3) (PDF)

AUTHOR INFORMATION

Corresponding Author

Noémie Janot − *Stanford Synchrotron Radiation Lightsource, SLAC National Accelerator Laboratory, Menlo Park, California 94025, United States;* Present Address: Noémie Janot: INRAE/Bordeaux Science Agro, ISPA, UMR 1391, 33882 Villenave d'Ornon, France; orcid.org/0000-0001-9287-2532; Email: noemie.janot@inrae.fr

Authors

Sarrah M. Dunham-Cheatham − *Stanford Synchrotron Radiation Lightsource, SLAC National Accelerator Laboratory, Menlo Park, California 94025, United States;* Present Address: Sarrah M. Dunham-Cheatham: College of Agriculture, Biotechnology & Natural Resources, University of Nevada, Reno, Nevada 89557, United States; orcid.org/0000-0002-2281-1686

Juan S. Lezama Pacheco − *Stanford Synchrotron Radiation Lightsource, SLAC National Accelerator Laboratory, Menlo Park, California 94025, United States;* Present Address: Juan S. Lezama Pacheco: Department of Environmental Earth System Science, Stanford University, Stanford, California 94305, United States

José M. Cerrato − *Department of Energy, Environmental, and Chemical Engineering, Washington University in St. Louis, St. Louis, Missouri 63130, United States;* Present Address: José M. Cerrato: Gerald May Department of Civil, Construction & Environmental Engineering, University of New Mexico, MSC01 1070, Albuquerque, New Mexico 87131, United States; orcid.org/0000-0002-2473-6376

Daniel S. Alessi − *Environmental Microbiology Laboratory, École Polytechnique Fédérale de Lausanne, CH-1015 Lausanne, Switzerland;* Present Address: Daniel S. Alessi: Department of Earth and Atmospheric Sciences, University of Alberta, Edmonton, Alberta T6G 2E3, Canada; orcid.org/0000-0002-8360-8251

Vincent Noël − *Stanford Synchrotron Radiation Lightsource, SLAC National Accelerator Laboratory, Menlo Park, California 94025, United States;* orcid.org/0000-0002-5387-8664

Eunmin Lee − *Department of Energy, Environmental, and Chemical Engineering, Washington University in St. Louis, St. Louis, Missouri 63130, United States*

Don Q. Pham − *Stanford Synchrotron Radiation Lightsource, SLAC National Accelerator Laboratory, Menlo Park, California 94025, United States*

Elena Suvorova − *Environmental Microbiology Laboratory, École Polytechnique Fédérale de Lausanne, CH-1015 Lausanne, Switzerland;* Present Address: Elena Suvorova: A.V. Shubnikov Institute of Crystallography, Federal Scientific Research Centre "Crystallography and Photonics" of the Russian Academy of Sciences, Leninsky Prospekt 59, Moscow 119333, Russia.

Rizlan Bernier-Latmani − *Environmental Microbiology Laboratory, École Polytechnique Fédérale de Lausanne, CH-1015 Lausanne, Switzerland;* orcid.org/0000-0001-6547-722X

Kenneth H. Williams − *Climate and Ecosystem Sciences Division, Lawrence Berkeley National Laboratory, Berkeley, California 94720, United States*

Philip E. Long − *Climate and Ecosystem Sciences Division, Lawrence Berkeley National Laboratory, Berkeley, California 94720, United States*

John R. Bargar − *Stanford Synchrotron Radiation Lightsource, SLAC National Accelerator Laboratory, Menlo Park, California 94025, United States;* Present Address: John R. Bargar: Environmental Molecular Sciences Laboratory, Pacific Northwest National Laboratory, Richland, Washington 99354, United States

Complete contact information is available at: https://pubs.acs.org/10.1021/acsearthspacechem.3c00271

Author Contributions

Noémie Janot, conceptualization, investigation, formal analysis, and writing—original draft; Sarrah M. Dunham-Cheatham, investigation and writing—review and editing; Juan S. Lezama Pacheco, conceptualization, formal analysis, and investigation; José M. Cerrato, investigation, formal analysis, and writing—review and editing; Daniel S. Alessi, investigation and writing—review and editing; Vincent Noël, investigation and writing—review and editing; Eunmin Lee, investigation; Don Q. Pham, investigation; Elena Suvorova, investigation; Rizlan Bernier-Latmani, conceptualization, methodology, supervision, project administration, funding acquisition, and writing—review and editing; Kenneth H. Williams, methodology, resources, project administration, funding acquisition, and writing—review and editing; Philip E. Long, project administration and funding acquisition; and John R. Bargar, conceptualization, methodology, validation, supervision, project administration, and funding acquisition.

Notes

The authors declare no competing financial interest.

ACKNOWLEDGMENTS

The authors thank Prof. Daniel E. Giammar for his help throughout this study, from conceptualization to project administration, and Sarah Morris (SM Stoller) for aqueous U analysis during the field experiment. Field operations, analyses, and salary support for Noémie Janot, Juan S. Lezama Pacheco, José M. Cerrato, Sarrah M. Dunham-Cheatham, Daniel S. Alessi, and John R. Bargar were provided by the SLAC Science Focus Area funded by the U.S. Department of Energy (DOE) Subsurface Biogeochemical Research program (FWP 10094). Additional funding was provided by the SLAC Floodplain Hydro-Biogeochemistry SFA program of the U.S. DOE, Office of Biological and Environmental Research, Earth and Environmental Systems Sciences Division under U.S. DOE Contract DE-AC02-76SF00515 (data analysis and writing). Portions of this research were carried out at the Stanford Synchrotron Radiation Lightsource, a national user facility operated by Stanford University on behalf of the U.S. DOE, Office of Basic Energy Sciences. The SSRL Structural Molecular Biology Program was supported by the U.S. DOE, Office of Biological and Environmental Research, and the National Institutes of Health, National Center for Research Resources, Biomedical Technology Program. The authors thank the SLAC radiation protection program for their assistance with radioactive sample handling. The Rifle IFRC site (Rifle, CO, U.S.A.) was supported by the U.S. DOE,

Biological and Environmental Research, Subsurface Biogeochemical Research program. Work carried out at EPFL was funded by Swiss NSF Grants 20021-113784 and 200020126821, SNSF International Co-operation Grant IZK0Z212355, and SNSF International Short Visits Grant IZK0Z2133214. Daniel S. Alessi was partially supported by a Marie Curie International Incoming Fellowship from the European Commission, Grant FP7-PEOPLE-2009-IIF254143. Contributions by the Lawrence Berkeley National Laboratory were supported through its Sustainable Systems Scientific Focus Area under Contract DE-AC02-05CH11231.

REFERENCES

(1) Smedley, P. L.; Kinniburgh, D. G. Uranium in Natural Waters and the Environment: Distribution, Speciation and Impact. *Appl. Geochem.* **2023**, *148*, No. 105534.

(2) Campbell, K. M.; Gallegos, T. J.; Landa, E. R. Biogeochemical Aspects of Uranium Mineralization, Mining, Milling, and Remediation. *Appl. Geochem.* **2015**, *57*, 206−235.

(3) Fuller, A. J.; Leary, P.; Gray, N. D.; Davies, H. S.; Mosselmans, J. F. W.; Cox, F.; Robinson, C. H.; Pittman, J. K.; McCann, C. M.; Muir, M.; Graham, M. C.; Utsunomiya, S.; Bower, W. R.; Morris, K.; Shaw, S.; Bots, P.; Livens, F. R.; Law, G. T. W. Organic Complexation of U(VI) in Reducing Soils at a Natural Analogue Site: Implications for Uranium Transport. *Chemosphere* **2020**, *254*, No. 126859.

(4) Shiel, A. E.; Johnson, T. M.; Lundstrom, C. C.; Laubach, P. G.; Long, P. E.; Williams, K. H. Reactive Transport of Uranium in a Groundwater Bioreduction Study: Insights from High-Temporal Resolution 238U/235U Data. *Geochim. Cosmochim. Acta* **2016**, *187*, 218−236.

(5) Williams, K. H.; Long, P. E.; Davis, J. A.; Wilkins, M. J.; N'Guessan, A. L.; Steefel, C. I.; Yang, L.; Newcomer, D.; Spane, F. A.; Kerkhof, L. J.; McGuinness, L.; Dayvault, R.; Lovley, D. R. Acetate Availability and Its Influence on Sustainable Bioremediation of Uranium-Contaminated Groundwater. *Geomicrobiol. J.* **2011**, *28* (5−6), 519−539.

(6) Lovley, D. R.; Phillips, E. J. P.; Gorby, Y. A.; Landa, E. R. Microbial Reduction of Uranium. *Nature* **1991**, *350*, 413−416.

(7) Fletcher, K. E.; Boyanov, M. I.; Thomas, S. H.; Wu, Q.; Kemner, K. M.; Löffler, F. E. U(VI) Reduction to Mononuclear U(IV) by Desulfitobacterium Species. *Environ. Sci. Technol.* **2010**, *44* (12), 4705−4709.

(8) Hyun, S. P.; Davis, J. A.; Sun, K.; Hayes, K. F. Uranium(VI) Reduction by Iron(II) Monosulfide Mackinawite. *Environ. Sci. Technol.* **2012**, *46* (6), 3369−3376.

(9) Latta, D. E.; Boyanov, M. I.; Kemner, K. M.; O'Loughlin, E. J.; Scherer, M. M. Abiotic Reduction of Uranium by Fe(II) in Soil. *Appl. Geochem.* **2012**, *27* (8), 1512−1524.

(10) Veeramani, H.; Scheinost, A. C.; Monsegue, N.; Qafoku, N. P.; Kukkadapu, R.; Newville, M.; Lanzirotti, A.; Pruden, A.; Murayama, M.; Hochella, M. F. Abiotic Reductive Immobilization of U(VI) by Biogenic Mackinawite. *Environ. Sci. Technol.* **2013**, *47* (5), 2361−2369.

(11) Bernier-Latmani, R.; Veeramani, H.; Vecchia, E. D.; Junier, P.; Lezama-Pacheco, J. S.; Suvorova, E. I.; Sharp, J. O.; Wigginton, N. S.; Bargar, J. R. Non-Uraninite Products of Microbial U(VI) Reduction. *Environ. Sci. Technol.* **2010**, *44* (24), 9456−9462.

(12) Stylo, M.; Alessi, D. S.; Shao, P. P.; Lezama-Pacheco, J. S.; Bargar, J. R.; Bernier-Latmani, R. Biogeochemical Controls on the Product of Microbial U(VI) Reduction. *Environ. Sci. Technol.* **2013**, *47* (21), 12351−12358.

(13) Zhang, L.; Chen, Y.; Xia, Q.; Kemner, K. M.; Shen, Y.; O'Loughlin, E. J.; Pan, Z.; Wang, Q.; Huang, Y.; Dong, H.; Boyanov, M. I. Combined Effects of Fe(III)-Bearing Clay Minerals and Organic Ligands on U(VI) Bioreduction and U(IV) Speciation. *Environ. Sci. Technol.* **2021**, *55* (9), 5929−5938.

(14) Loreggian, L.; Novotny, A.; Bretagne, S. L.; Bartova, B.; Wang, Y.; Bernier-Latmani, R. Effect of Aging on the Stability of Microbially-Reduced Uranium in Natural Sediments. *Environ. Sci. Technol.* **2020**, *54* (1), 613−620.

(15) Cerrato, J. M.; Ashner, M. N.; Alessi, D. S.; Lezama-Pacheco, J. S.; Bernier-Latmani, R.; Bargar, J. R.; Giammar, D. E. Relative Reactivity of Biogenic and Chemogenic Uraninite and Biogenic Noncrystalline U(IV). *Environ. Sci. Technol.* **2013**, *47* (17), 9756−9763.

(16) Bi, Y.; Stylo, M.; Bernier-Latmani, R.; Hayes, K. F. Rapid Mobilization of Noncrystalline U(IV) Coupled with FeS Oxidation. *Environ. Sci. Technol.* **2016**, *50* (3), 1403−1411.

(17) Chardi, K. J.; Satpathy, A.; Schenkeveld, W. D. C.; Kumar, N.; Noël, V.; Kraemer, S. M.; Giammar, D. E. Ligand-Induced U Mobilization from Chemogenic Uraninite and Biogenic Noncrystalline U(IV) under Anoxic Conditions. *Environ. Sci. Technol.* **2022**, *56* (10), 6369−6379.

(18) Dwivedi, D.; Steefel, C. I.; Arora, B.; Banfield, J.; Bargar, J.; Boyanov, M. I.; Brooks, S. C.; Chen, X.; Hubbard, S. S.; Kaplan, D.; Kemner, K. M.; Nico, P. S.; O'Loughlin, E. J.; Pierce, E. M.; Painter, S. L.; Scheibe, T. D.; Wainwright, H. M.; Williams, K. H.; Zavarin, M. From Legacy Contamination to Watershed Systems Science: A Review of Scientific Insights and Technologies Developed through DOE-Supported Research in Water and Energy Security. *Environ. Res. Lett.* **2022**, *17* (4), No. 043004.

(19) Anderson, R. T.; Vrionis, H. A.; Ortiz-Bernad, I.; Resch, C. T.; Long, P. E.; Dayvault, R.; Karp, K.; Marutzky, S.; Metzler, D. R.; Peacock, A.; White, D. C.; Lowe, M.; Lovley, D. R. Stimulating the In Situ Activity of Geobacter Species To Remove Uranium from the Groundwater of a Uranium-Contaminated Aquifer. *Appl. Environ. Microbiol.* **2003**, *69* (10), 5884−5891.

(20) Watson, D. B.; Wu, W.-M.; Mehlhorn, T.; Tang, G.; Earles, J.; Lowe, K.; Gihring, T. M.; Zhang, G.; Phillips, J.; Boyanov, M. I.; Spalding, B. P.; Schadt, C.; Kemner, K. M.; Criddle, C. S.; Jardine, P. M.; Brooks, S. C. In Situ Bioremediation of Uranium with Emulsified Vegetable Oil as the Electron Donor. *Environ. Sci. Technol.* **2013**, *47* (12), 6440−6448.

(21) Wu, W.-M.; Carley, J.; Fienen, M.; Mehlhorn, T.; Lowe, K.; Nyman, J.; Luo, J.; Gentile, M. E.; Rajan, R.; Wagner, D.; Hickey, R. F.; Gu, B.; Watson, D.; Cirpka, O. A.; Kitanidis, P. K.; Jardine, P. M.; Criddle, C. S. Pilot-Scale in Situ Bioremediation of Uranium in a Highly Contaminated Aquifer. 1. Conditioning of a Treatment Zone. *Environ. Sci. Technol.* **2006**, *40* (12), 3978−3985.

(22) Alessi, D. S.; Lezama-Pacheco, J. S.; Janot, N.; Suvorova, E. I.; Cerrato, J. M.; Giammar, D. E.; Davis, J. A.; Fox, P. M.; Williams, K. H.; Long, P. E.; Handley, K. M.; Bernier-Latmani, R.; Bargar, J. R. Speciation and Reactivity of Uranium Products Formed during *in Situ* Bioremediation in a Shallow Alluvial Aquifer. *Environ. Sci. Technol.* **2014**, *48* (21), 12842−12850.

(23) Long, P. E.; Williams, K. H.; Davis, J. A.; Fox, P. M.; Wilkins, M. J.; Yabusaki, S. B.; Fang, Y.; Waichler, S. R.; Berman, E. S. F.; Gupta, M.; Chandler, D. P.; Murray, C.; Peacock, A. D.; Giloteaux, L.; Handley, K. M.; Lovley, D. R.; Banfield, J. F. Bicarbonate Impact on U(VI) Bioreduction in a Shallow Alluvial Aquifer. *Geochim. Cosmochim. Acta* **2015**, *150*, 106−124.

(24) Xu, J.; Veeramani, H.; Qafoku, N. P.; Singh, G.; Riquelme, M. V.; Pruden, A.; Kukkadapu, R. K.; Gartman, B. N.; Hochella, M. F. Efficacy of Acetate-Amended Biostimulation for Uranium Sequestration: Combined Analysis of Sediment/Groundwater Geochemistry and Bacterial Community Structure. *Appl. Geochem.* **2017**, *78*, 172−185.

(25) Yabusaki, S. B.; Fang, Y.; Williams, K. H.; Murray, C. J.; Ward, A. L.; Dayvault, R. D.; Waichler, S. R.; Newcomer, D. R.; Spane, F. A.; Long, P. E. Variably Saturated Flow and Multicomponent Biogeochemical Reactive Transport Modeling of a Uranium Bioremediation Field Experiment. *J. Contam. Hydrol.* **2011**, *126* (3−4), 271−290.

(26) Li, L.; Gawande, N.; Kowalsky, M. B.; Steefel, C. I.; Hubbard, S. S. Physicochemical Heterogeneity Controls on Uranium Bioreduction Rates at the Field Scale. *Environ. Sci. Technol.* **2011**, *45* (23), 9959−9966.

https://doi.org/10.1021/acsearthspacechem.3c00271
ACS Earth Space Chem. 2024, 8, 148−158

(27) Jemison, N. E.; Bizjack, M. T.; Johnson, T. M.; Druhan, J. L. Influence of Physical and Chemical Hydrology on Bioremediation of a U-Contaminated Aquifer Informed by Reactive Transport Modeling Incorporating $^{238}U/^{235}U$ Ratios. *Geochim. Cosmochim. Acta* **2020**, *269*, 303−328.
(28) Bargar, J. R.; Williams, K. H.; Campbell, K. M.; Long, P. E.; Stubbs, J. E.; Suvorova, E. I.; Lezama Pacheco, J. S.; Alessi, D. S.; Stylo, M.; Webb, S. M.; Davis, J. A.; Giammar, D. E.; Blue, L. Y.; Bernier-Latmani, R. Uranium Redox Transition Pathways in Acetate-Amended Sediments. *Proc. Natl. Acad. Sci. U. S. A.* **2013**, *110* (12), 4506−4511.
(29) Stylo, M.; Neubert, N.; Roebbert, Y.; Weyer, S.; Bernier-Latmani, R. Mechanism of Uranium Reduction and Immobilization in *Desulfovibrio Vulgaris* Biofilms. *Environ. Sci. Technol.* **2015**, *49* (17), 10553−10561.
(30) Latta, D. E.; Mishra, B.; Cook, R. E.; Kemner, K. M.; Boyanov, M. I. Stable U(IV) Complexes Form at High-Affinity Mineral Surface Sites. *Environ. Sci. Technol.* **2014**, *48* (3), 1683−1691.
(31) Boyanov, M. I.; Fletcher, K. E.; Kwon, M. J.; Rui, X.; O'Loughlin, E. J.; Löffler, F. E.; Kemner, K. M. Solution and Microbial Controls on the Formation of Reduced U(IV) Species. *Environ. Sci. Technol.* **2011**, *45* (19), 8336−8344.
(32) Boyanov, M. I.; Latta, D. E.; Scherer, M. M.; O'Loughlin, E. J.; Kemner, K. M. Surface Area Effects on the Reduction of UVI in the Presence of Synthetic Montmorillonite. *Chem. Geol.* **2017**, *464*, 110−117.
(33) Loreggian, L.; Sorwat, J.; Byrne, J. M.; Kappler, A.; Bernier-Latmani, R. Role of Iron Sulfide Phases in the Stability of Noncrystalline Tetravalent Uranium in Sediments. *Environ. Sci. Technol.* **2020**, *54* (8), 4840−4846.
(34) Alessi, D. S.; Uster, B.; Veeramani, H.; Suvorova, E. I.; Lezama-Pacheco, J. S.; Stubbs, J. E.; Bargar, J. R.; Bernier-Latmani, R. Quantitative Separation of Monomeric U(IV) from UO_2 in Products of U(VI) Reduction. *Environ. Sci. Technol.* **2012**, *46* (11), 6150−6157.
(35) Prietzel, J.; Botzaki, A.; Tyufekchieva, N.; Brettholle, M.; Thieme, J.; Klysubun, W. Sulfur Speciation in Soil by S K-Edge XANES Spectroscopy: Comparison of Spectral Deconvolution and Linear Combination Fitting. *Environ. Sci. Technol.* **2011**, *45* (7), 2878−2886.
(36) Webb, S. M. SIXPack: A Graphical User Interface for XAS Analysis Using IFEFFIT. *Phys. Scr.* **2005**, *2005*, 1011.
(37) Ravel, B.; Newville, M. ATHENA, ARTEMIS, HEPHAESTUS: Data Analysis for X-ray Absorption Spectroscopy Using IFEFFIT. *J. Synchrotron Radiat.* **2005**, *12*, 537−541.
(38) Newville, M. Larch: An Analysis Package for XAFS and Related Spectroscopies. *J. Phys.: Conf. Ser.* **2013**, *430* (1), No. 012007.
(39) Noël, V.; Boye, K.; Kukkadapu, R. K.; Bone, S.; Lezama Pacheco, J. S.; Cardarelli, E.; Janot, N.; Fendorf, S.; Williams, K. H.; Bargar, J. R. Understanding Controls on Redox Processes in Floodplain Sediments of the Upper Colorado River Basin. *Sci. Total Environ.* **2017**, *603−604*, 663−675.
(40) Schofield, E. J.; Veeramani, H.; Sharp, J. O.; Suvorova, E.; Bernier-Latmani, R.; Mehta, A.; Stahlman, J.; Webb, S. M.; Clark, D. L.; Conradson, S. D.; Ilton, E. S.; Bargar, J. R. Structure of Biogenic Uraninite Produced by *Shewanella oneidensis* Strain MR-1. *Environ. Sci. Technol.* **2008**, *42* (21), 7898−7904.
(41) Singer, D. M.; Farges, F.; Brown, G. E. Biogenic Nanoparticulate UO_2: Synthesis, Characterization, and Factors Affecting Surface Reactivity. *Geochim. Cosmochim. Acta* **2009**, *73* (12), 3593−3611.
(42) Webb, S. M. The MicroAnalysis Toolkit: X-ray Fluorescence Image Processing Software. *AIP Conf. Proc.* **2011**, *1365*, 196−199.
(43) Druhan, J. L.; Steefel, C. I.; Molins, S.; Williams, K. H.; Conrad, M. E.; DePaolo, D. J. Timing the Onset of Sulfate Reduction over Multiple Subsurface Acetate Amendments by Measurement and Modeling of Sulfur Isotope Fractionation. *Environ. Sci. Technol.* **2012**, *46* (16), 8895−8902.
(44) Callister, S. J.; Wilkins, M. J.; Nicora, C. D.; Williams, K. H.; Banfield, J. F.; VerBerkmoes, N. C.; Hettich, R. L.; N'Guessan, A. L.; Mouser, P. J.; Elifantz, H.; Smith, R. D.; Lovley, D. R.; Lipton, M. S.; Long, P. E. Analysis of Biostimulated Microbial Communities from Two Field Experiments Reveals Temporal and Spatial Differences in Proteome Profiles. *Environ. Sci. Technol.* **2010**, *44* (23), 8897−8903.
(45) Bone, S. E.; Dynes, J. J.; Cliff, J.; Bargar, J. R. Uranium(IV) Adsorption by Natural Organic Matter in Anoxic Sediments. *Proc. Natl. Acad. Sci. U. S. A.* **2017**, *114* (4), 711−716.
(46) Ulrich, K.-U.; Veeramani, H.; Bernier-Latmani, R.; Giammar, D. E. Speciation-Dependent Kinetics of Uranium(VI) Bioreduction. *Geomicrobiol. J.* **2011**, *28* (5−6), 396−409.
(47) Xie, J.; Wang, J.; Lin, J. New Insights into the Role of Calcium in the Bioreduction of Uranium(VI) under Varying pH Conditions. *J. Hazard. Mater.* **2021**, *411*, No. 125140.
(48) Bao, C.; Wu, H.; Li, L.; Newcomer, D.; Long, P. E.; Williams, K. H. Uranium Bioreduction Rates across Scales: Biogeochemical Hot Moments and Hot Spots during a Biostimulation Experiment at Rifle, Colorado. *Environ. Sci. Technol.* **2014**, *48* (17), 10116−10127.
(49) Komlos, J.; Moon, H. S.; Jaffé, P. R. Effect of Sulfate on the Simultaneous Bioreduction of Iron and Uranium. *J. Environ. Qual.* **2008**, *37* (6), 2058.
(50) Behrends, T.; Van Cappellen, P. Competition between Enzymatic and Abiotic Reduction of Uranium(VI) under Iron Reducing Conditions. *Chem. Geol.* **2005**, *220* (3−4), 315−327.
(51) Chao, T. T.; Zhou, L. Extraction Techniques for Selective Dissolution of Amorphous Iron-Oxides Form Soils and Sediments. *Soil Sci. Soc. Am. J.* **1983**, *47* (2), 225−232.
(52) Wilkins, M. J.; Callister, S. J.; Miletto, M.; Williams, K. H.; Nicora, C. D.; Lovley, D. R.; Long, P. E.; Lipton, M. S. Development of a Biomarker for Geobacter Activity and Strain Composition; Proteogenomic Analysis of the Citrate Synthase Protein during Bioremediation of U(VI): Geobacter Citrate Synthase Biomarker. *Microb. Biotechnol.* **2011**, *4* (1), 55−63.
(53) Mikutta, C.; Langner, P.; Bargar, J. R.; Kretzschmar, R. Tetra- and Hexavalent Uranium Forms Bidentate-Mononuclear Complexes with Particulate Organic Matter in a Naturally Uranium-Enriched Peatland. *Environ. Sci. Technol.* **2016**, *50* (19), 10465−10475.